ing Aspects of MHD, Argonne, IL, 1972.
[2]Blom, J. H., Veefkind, A., and Reitjens, L. H. Th., "High Power Density Experiments in the Eindhoven Shocktunnel MHD Generator," 6th International Conf. on MHD Electrical Power Generation, Washington, DC, 1975.
[3]Heydt, R. P., "The Effect of Rod Electrodes on the Performance of Combustion MHD Generators," Ph.D. Dissertation, Dept. of Mechanical Engineering, Stanford Univ., Stanford, CA, Oct. 1985.

Combustion Performance of Bipropellant Liquid Rocket Engine Combustors with Fuel-Impingement Cooling

Tsung Leo Jiang* and Wei-Tang Chiang†
National Cheng Kung University, Tainan, Taiwan 70101, Republic of China
and
Shyh-Dihng Jang‡
Lungtan, Taiwan 32526, Republic of China

Introduction

A NUMBER of computational fluid dynamics (CFD) approach-based comprehensive analytical tools have been recently proposed in providing detailed combustion analyses and in aiding in the thruster design of the modern advanced liquid rocket engine. For instance, Liang et al.[1] successfully analyzed a cryogenic LOX/H_2 rocket engine combustor with a liquid-gas injection. Jiang and Chiu,[2] however, proposed a computational bipropellant spray combustion model, in which both fuel and oxidizer droplet flows were solved, and when certain droplet combustion criteria were satisfied, fuel or oxidizer droplet burning was assumed. Their numerical predictions[2] revealed that finer-droplet sprays do not necessarily lead to a higher combustion efficiency as traditionally speculated. The bipropellant spray combustion model was also applied in analyzing an orbital maneuvering vehicle's (OMV) thrust chamber.[3] This chamber was equipped with a centrally installed pintle-type ring-shaped injector. For such a small in-space propulsive engine combustor, the propellant conversion efficiency was predicted to be relatively low due to poor bipropellant mixing resulting from part of the fuel being injected toward the chamber wall for impingement cooling.

Due to the complexity associated with modeling the expansion nozzle, numerical analyses of liquid bipropellant rocket engine combustors have unanimously been confined within the combustor itself, thereby allowing the effects of the nozzle to be neglected with the chamber pressure being specified as a prior given condition at a point on the injector face. However, the combustion performance of a bipropellant liquid rocket engine thruster can be evaluated only when the chamber pressure is predicted rather than prespecified. Therefore, the flow analysis has to be conducted from the injector face down to at least the propulsive nozzle throat. In the present study, the flow analysis for the axisymmetric thrust chamber of an OMV[3] installed with a pintle-type ring-shaped injector and a conical convergent nozzle is conducted. Liquid monomethyl hydrazine (MMH) and nitrogen tetroxide (NTO) storable bipropellants serve as the fuel and oxidizer sources, respectively, with MMH being assumed injected through the injector toward the chamber wall for impingement cooling. An optimum injected fuel and oxidizer droplet-size combination is suggested based upon the results obtained from a systematic sensitivity study examining the effects of both injected fuel and oxidizer droplet sizes on chamber-wall temperature distributions and the chamber pressure.

Received May 29, 1993; revision received July 14, 1994; accepted for publication Oct. 6, 1994.
*Associate Professor, Institute of Aeronautics and Astronautics.
†Research Assistant, Institute of Aeronautics and Astronautics.
‡Senior Scientist, P.O. Box 90008-15-12. Member AIAA.

Formulation

The present mathematical framework consists of an Eulerian/Eulerian approach[2,3] for gas and liquid-droplet flows. The full axisymmetric compressible Navier-Stokes equations as well as the compressible k-ε two-equation turbulence model are solved for the gas flow. The liquid-droplet flow equations for each droplet-size group consist of the droplet number-density, momentum, and energy equations. For fuel and oxidizer, the inlet droplet number density is assumed to linearly decrease and increase, respectively, as one goes from the outer to the inner rim of the pintle-type ring-shaped injector. With such an injection pattern, fuel impingement cooling at the chamber wall is viable. The choking condition is assumed at the nozzle throat. For such an irregularly shaped combustor, a computer code[4] was specially developed based on body-fitted nonorthogonal grids and employed in analyzing the present compressible turbulent reacting flow. The computational geometric configuration and grid system consisting of 48 × 21 nonuniform staggered grids are depicted in Fig. 1. Convergence is assured by requiring the maximum mass residual of the continuity equation down to prescribed small values and the relative difference of the variables between two iterations smaller than 10^{-4}. More than 3000 iterations are required for a converged calculation.

Results and Discussion

In the present analysis, a fuel-rich injection ratio of 1.64 is presumed, since part of the fuel is assumed to be injected toward the chamber wall for impingement cooling. The ratio of nozzle inlet to throat area is 6.637, and the total mass flow rate is 0.2133 kg/s. The variation in chamber pressure predicted for various injected fuel and oxidizer volume-mean droplet diameters (D_{30}) is depicted in Fig. 2. Chamber pressure is defined as the mean pressure at the injector face. Injected droplet size combinations of 20, 40, 60, 80, and 100 μm and 40, 60, 80, and 100 μm are investigated for $(D_{30})_{ox}$ and $(D_{30})_{fu}$, respectively. For each $(D_{30})_{ox}$ series [different $(D_{30})_{fu}$ values for a constant $(D_{30})_{ox}$ value], best performance in terms of maximum chamber pressure results for the following various $(D_{30})_{fu}$: $40 > 60 > 80 > 100$ μm, except for the 100-μm $(D_{30})_{ox}$ series, where a $(D_{30})_{fu}$ of 80 μm yields the maximum chamber pressure. It is interesting to note that for each $(D_{30})_{fu}$, increasing $(D_{30})_{ox}$ results in a marked increase in chamber pressure to a maximum value at a $(D_{30})_{ox}$ of 80 μm, after which, chamber pressure drops off slowly. This result indicates that for the present thrust chamber and injection pattern, there exists an optimum $(D_{30})_{ox}$ value that achieves the best combustion performance. Excessively small $(D_{30})_{ox}$, however, generally lead to low combustion performance.

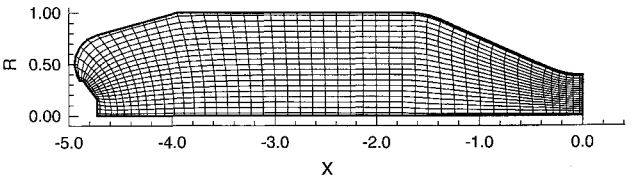

Fig. 1 Computational geometric configuration and grid system of the combustor.

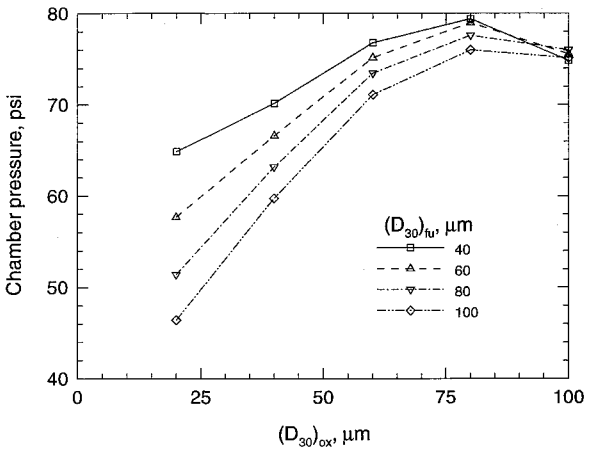

Fig. 2 Predicted chamber pressure vs injected $(D_{30})_{ox}$ under various injected $(D_{30})_{fu}$.

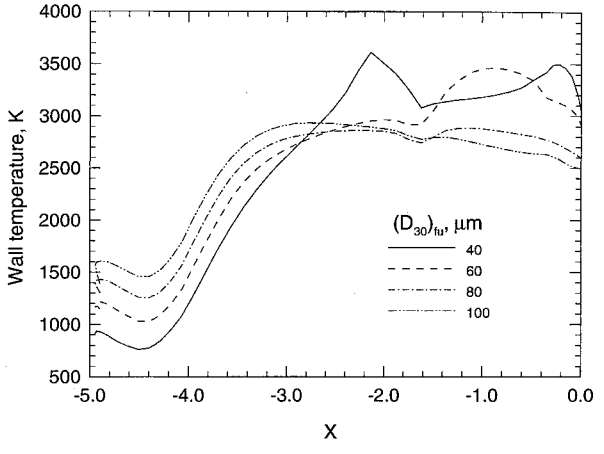

Fig. 3 Chamber wall temperature distribution at a constant $(D_{30})_{ox}$ of 80 μm and $(D_{30})_{fu}$ of 40, 60, 80, and 100 μm.

For a large oxidizer droplet injection, due to their size, oxidizer droplets are able to flow from the inner oxidizer-rich zone into the outer fuel-rich zone, resulting in high combustion performance due to both outer-region and inner broad-zone combustion. For a small oxidizer droplet injection, on the other hand, the majority of oxidizer droplets vaporize completely before flowing into the outer fuel-rich region, inducing an intense interflame in the region between the fuel- and oxidizer-rich zones. It blocks outer-zone fuel vapor from diffusing into the inner zone, preventing fuel and oxidizer mixing. As a result, fuel and oxidizer vapor remain unmixed and flow with the stream of combustion products, leading to poor utilization of the combustor and low combustion performance. Excessively large oxidizer droplets, however, do not promote fast combustion, since their gasification rates are substantially lower than those of their smaller-sized counterparts. Therefore, the size of an injected oxidizer droplet for the highest combustion performance should be large enough to excite broad combustion zones, while small enough to vaporize or burn quickly, thereby promoting fast combustion.

As for injected fuel-droplet size effects, chamber pressure increases within each $(D_{30})_{ox}$ with decreasing $(D_{30})_{fu}$, except for a $(D_{30})_{ox}$ of 100 μm, where a $(D_{30})_{fu}$ of 80 μm yields the maximum chamber pressure (Fig. 2). Fuel vapor released relatively quickly from small injected fuel droplets not only enhances combustion of oxidizer droplets/vapor flowing from the inner to the outer region, but also excites inner oxidizer droplet/vapor burning, increasing the overall combustion performance. Slow vaporization rates of large fuel droplets, on the other hand, fail to excite an inner burning zone, with combustion occurring mainly in the outer region, yielding a relatively lower chamber pressure. For a substantially large $(D_{30})_{ox}$ of 100 μm, part of oxidizer droplets flow into, and accumulate around, the midregion and the convergent-nozzle section of the combustor, resulting in a locally oxidizer-rich region therein. As large injected fuel droplets may not vaporize completely before leaving the nozzle, they possess a better chance of burning in the downstream region of the combustor. These two opposite effects of a slower vaporization rate, but an increased opportunity to burn lead to the observed maximum pressure occurring for the $(D_{30})_{fu}$ = 80 μm and $(D_{30})_{ox}$ = 100 μm injection condition. The chamber pressure for this injection combination is, however, still lower than that of $(D_{30})_{fu}$ = 80 μm and $(D_{30})_{ox}$ = 80 μm, due to the former's excessively large oxidizer droplets.

Temperature distributions along the chamber wall are presented in Fig. 3 for various $(D_{30})_{fu}$ droplet sizes at a constant $(D_{30})_{ox}$ of 80 μm. The latter value corresponds to the optimum injected $(D_{30})_{ox}$ that yielded the maximum chamber pressure within each $(D_{30})_{fu}$ in Fig. 2. For a large $(D_{30})_{fu}$ injection (100 μm), chamber wall temperature reaches approximately 2950 K in the midregion of the combustor, since a small number of larger fuel droplets absorb less heat from combustion than do a large number of smaller fuel droplets. In the nozzle section, since large $(D_{30})_{fu}$ injections (80 and 100 μm) still possess sufficient fuel droplets therein for cooling purposes, the chamber wall is accordingly kept at a slightly lower temperature (around 2700 K). Chamber-wall temperatures in excess of 3500 K result for both 40 and 60 μm $(D_{30})_{fu}$ injections. For various oxidizer droplet sizes at a constant $(D_{30})_{fu}$ of 40 μm, the maximum chamber wall temperature for a 20 μm $(D_{30})_{ox}$ is relatively lower, since the mixing of small oxidizer droplets with outer fuel vapor and fuel droplets is poor under the present partially nonpremixed injection configuration. The 80- and 100-μm $(D_{30})_{ox}$ cases, however, exhibit very high maximum chamber-wall temperatures above 3500 K (not shown), since both fuel droplet and gas combustion are locally excited. The 60 μm $(D_{30})_{ox}$ injection condition, on the other hand, exhibits a chamber-wall temperature remaining below 2500 K.

The prime criterion in determining an optimum $(D_{30})_{fu}$, $(D_{30})_{ox}$ injection condition is keeping the chamber wall below its upper temperature limit, thereby preventing engine meltdown. The upper temperature limit, however, depends mainly upon the materials used for the chamber wall. For instance, if this limit is 3500 K, the 80 μm $(D_{30})_{ox}$ and 40 μm $(D_{30})_{fu}$ injection condition, demonstrating the highest combustion performance among the present investigated injection conditions, is not appropriate due to the fact that chamber wall temperatures in excess of 3600 K result in the downstream region of the combustor. Although the 80 μm $(D_{30})_{ox}$ and 60 μm $(D_{30})_{fu}$ injection condition results in the second highest chamber pressure, this case is, at best, marginal, since chamber wall temperatures approaching 3500 K occur in the nozzle section. For a chamber wall temperature limit of 3500 K, the 80 μm $(D_{30})_{ox}$ and 80 μm $(D_{30})_{fu}$ injection condition represents the best choice, since it results in the third highest chamber pressure while maintaining chamber wall temperatures below 3000 K. For a chamber wall temperature limit of 3000 K, the 60 μm $(D_{30})_{ox}$ and 40 μm $(D_{30})_{fu}$ injection condition is optimal, since it results in a chamber pressure just slightly lower than that resulting from the 80 μm $(D_{30})_{ox}$ and 80 μm $(D_{30})_{fu}$ injection condition, while maintaining chamber wall temperatures below 2500 K.

Conclusions

The chamber pressure of a storable bipropellant liquid rocket engine combustor with fuel impingement cooling was predicted numerically under various fuel and oxidizer droplet-size injection conditions: $(D_{30})_{fu}$ = 40, 60, 80, and 100 μm

and $(D_{30})_{ox}$ = 20, 40, 60, 80, and 100 μm. Under the present investigated injected droplet size combinations, an optimum injected oxidizer droplet size of $(D_{30})_{ox}$ = 80 μm existed, yielding a maximum chamber pressure for each investigated injected fuel droplet size. Small injected fuel droplet sizes lead to a high chamber pressure, except for a $(D_{30})_{ox}$ of 100 μm, where a $(D_{30})_{fu}$ of 80 μm leads to a maximum chamber pressure. An injected fuel and oxidizer droplet-size combination corresponding to a maximum chamber pressure occurred for a $(D_{30})_{fu}$ and a $(D_{30})_{ox}$ of 40 and 80 μm, respectively. For an assumed 3500 K upper temperature limit of the chamber wall, the $(D_{30})_{ox}$ = 80 μm and $(D_{30})_{fu}$ = 80 μm injection combination is suggested based not only upon a high chamber pressure, but also upon a sufficiently low chamber-wall temperature. For a lower chamber-wall temperature limit of 3000 K, the $(D_{30})_{ox}$ = 60 μm and $(D_{30})_{fu}$ = 40 μm injection condition represented the best choice. An optimal fuel and oxidizer droplet-size injection combination is thus determined based not only upon a high achieved chamber pressure, but also on a sufficiently cool chamber wall, where the maximum temperature is safely below the chamber wall's upper temperature limit. Fuel and oxidizer droplet sizes are thus selected at their optimum values rather than "as fine as possible" as in conventional design.

References

[1]Liang, P. Y., Fisher, S., and Chang, Y. M., "Comprehensive Modeling of a Liquid Rocket Combustion Chamber," *Journal of Propulsion and Power*, Vol. 2, No. 2, 1986, pp. 97–104.

[2]Jiang, T. L., and Chiu, H. H., "Bipropellant Combustion in a Liquid Propellant Rocket Combustion Chamber," *Journal of Propulsion and Power*, Vol. 8, No. 5, 1992, pp. 995–1003.

[3]Chiu, H. H., Jiang, T. L., Krebsbach, A. N., and Gross, K. W., "Numerical Analysis of Bipropellant Combustion in Orbital Maneuvering Vehicle Thrust Chamber," AIAA Paper 90-0045, Jan. 1990.

[4]Jiang, T. L., "The Flow Computation of a Liquid Rocket Engine Combustor of Complex Geometry," 12th International Conf. on Numerical Methods in Fluid Dynamics, 1990.

Efficient Mapping Topology for Turbine Combustors with Inclined Slots/Staggered Holes

S. L. Yang*
Michigan Technological University, Houghton, Michigan 49931-1295
and
M. C. Cline†
Los Alamos National Laboratory, Los Alamos, New Mexico 87545

Introduction

In many gas-turbine combustor applications, design of the dilution zone is an important factor for the success of the combustor. There are different configurations for introducing the dilution air into the combustor; the most commonly used geometry is dilution holes. The dilution holes may be arranged as a single row or multiple rows with in-line and/or staggered structures. For some combustors, inclined slots are used.[1–4]

The development of the high-speed digital computer makes numerical simulations of gas-turbine combustors more attainable.[3–6] To simulate the fluid flow and heat transfer occurring inside the combustor numerically, a grid system must be set up first. It is desirable to have a smaller physical region, if possible, so that a higher grid density can be formed, compared to a larger physical domain with the same number of grid points used to generate the mesh.

The purpose of this Note is to present an efficient grid generation topology for generating grid systems for gas-turbine combustors with inclined slots or staggered holes. In the subsequent sections, the ideal of choosing a smaller physical domain for setting up the mesh, the effect of this choice on the boundary conditions, the scheme to generate the mesh, and the effect of this mesh on the numerical solution are presented. For the purpose of this presentation, a gas-turbine combustor with inclined slots is used as an example.

Inclined Slots Example

Figure 1 shows a staged turbine combustor (STC) that consists of a fuel nozzle, a rich-burn (RB) zone, a quick-quench (QQ) zone, and a lean-combustion (LC) zone. Combustion is initiated in the RB zone. The hot rich mixture is then rapidly diluted and mixed by an array of air dilution slots in the QQ zone. The combustion is completed in the LC zone. Details of this combustor can be found in Refs. 1–4.

The focus here will be on the QQ/LC region of the STC shown in Fig. 1. As mentioned, in this region cool dilution air is injected into the QQ zone through inclined slots. Figure 1 also shows the section view of the QQ/LC region, where R is the radius and L is the length. There are eight, equally spaced inclined slots located around the perimeter of the QQ zone. Due to geometric symmetry, only one slot is modeled, resulting in a 45-deg sector. The slot is located at the center of the sector.

Mapping Topology

To generate a grid system for the configuration just described, Figs. 2a and 2b show two possible choices for selecting the two transverse boundaries shown in Fig. 1 to form the physical domain. Figure 2a shows the transverse boundaries (dashed lines) that are selected as horizontal lines in the axial direction. In Fig. 2b, the transverse boundaries are aligned to the direction of the inclined slot. The periodic boundary condition may be used at the transverse boundaries for both cases. By inspection, it is clear that Fig. 2b will give a smaller physical domain for the numerical solution.

In addition to the undesirability of a larger physical domain, two additional drawbacks may also be created by using Fig. 2a's option. As shown in Fig. 3, it is not an easy task to maintain good grid quality for this choice. This is mainly due to the orientation of the inclined slot. For the case of large aspect ratio (defined as the ratio of length to width) slots, the slots may be overlapped as indicated in Fig. 2c. From this figure, one can see that the simple periodic boundary condition is no longer valid at the transverse boundaries. In fact, how to select and apply the boundary condition at these two boundaries becomes a nontrivial problem.

For all these reasons, Fig. 2b's structure should be used. The immediate question is how to efficiently generate the mesh for this arrangement. This is described in the next section.

Grid Generation Scheme

To generate a grid using Fig. 2b, an efficient and simple grid-generation scheme has been developed. This grid-generation scheme involves two major steps. First, a three-di-

Received Aug. 14, 1993; revision received Sept. 26, 1994; accepted for publication Sept. 26, 1994.

*Assistant Professor, ME-EM Department. Member AIAA.

†Technical Staff Member, Group T-3 (Theoretical Fluid Dynamics). Member AIAA.